Linear polarization study of microwave-radiation-induced magnetoresistance oscillations: Comparison of power dependence to theory

Tianyu Ye,[1] Jesús Iñarrea,[2,3] W. Wegscheider,[4] and R. G. Mani[1]
[1]*Department of Physics and Astronomy, Georgia State University, Atlanta, Georgia 30303, USA*
[2]*Escuela Politécnica Superior, Universidad Carlos III, Leganes, Madrid 28911, Spain*
[3]*Unidad Asociada al Instituto de Ciencia de Materiales, CSIC, Cantoblanco, Madrid 28049, Spain*
[4]*Laboratorium für Festkörperphysik, ETH Zürich, 8093 Zürich, Switzerland*
(Received 16 May 2016; published 25 July 2016)

We present an experimental study of the microwave power and the linear polarization angle dependence of the microwave-induced magnetoresistance oscillations in the high-mobility GaAs/AlGaAs two-dimensional electron system. Experimental results show the sinusoidal dependence of the oscillatory magnetoresistance extrema as a function of the polarization angle. Yet, as the microwave power increases, the angular dependence includes additional harmonic content, and it begins to resemble the absolute value of the cosine function. We present a theory to explain such peculiar behavior.

DOI: 10.1103/PhysRevB.94.035305

I. INTRODUCTION

Microwave-radiation-induced zero-resistance states [1,2] are an interesting phenomenon in two-dimensional electron systems (2DES) because, for example, the coincidence of microwave-induced zero-resistance states with quantum Hall zero-resistance states leads to the extinction of the associated quantum Hall plateaus [3]. The microwave-radiation-induced magnetoresistance oscillations that lead to the zero-resistance states include characteristic traits such as periodicity in B^{-1} [1,2], a 1/4-cycle shift [4], distinctive sensitivity to temperature and microwave power [5,6], along with other specific features [7–33]. The linear-polarization sensitivity of these oscillations has been a topic of intensive recent experimental study [13,17,23,26,28,34,35]; these studies have shown that the amplitude of microwave-radiation-induced magnetoresistance oscillations changes periodically with the linear microwave polarization angle.

Looking at the linear polarization characteristics in greater detail, at fixed temperature and polarization angle the amplitude of microwave-radiation-induced magnetoresistance oscillations increases with the microwave power. It follows that, approximately [5,6], $A = A_0 P^{\alpha}$, where A is the amplitude of microwave-radiation-induced magnetoresistance oscillations, A_0 and $\alpha \approx 1/2$ are constants, and P is the microwave power. At fixed temperature and microwave power, the amplitude of microwave-radiation-induced magnetoresistance oscillations changes sinusoidally with the linear polarization angle. The experimental results have shown that the longitudinal resistance R_{xx} versus linear polarization angle θ follows a cosine square function [17], i.e., $R_{xx}(\theta) = A \pm C\cos^2(\theta - \theta_0)$ (A and C are constants and θ_0 is the phase shift, all of which depend on microwave frequency [27]), at low microwave power. Note that this angular dependence can also be rewritten as $R_{xx}(\theta) = A \pm (C/2)\{1 + \cos[2(\theta - \theta_0)]\}$. Deviation from this functional form was noted for higher microwave intensities.

From a theoretical point of view [36–54], there are many approaches to understand the physics of the microwave-radiation-induced magnetoresistance oscillations. These include the radiation-assisted indirect inter-Landau-level scattering by phonons and impurities (the displacement model) [36,40], the periodic motion of the electron orbit centers under irradiation (the radiation-driven electron orbit model) [41], and a radiation-induced steady-state nonequilibrium distribution (the inelastic model) [42]. Among these approaches, the radiation-driven electron orbit model intensively considered temperature [55,56], microwave power [6], and microwave polarization direction [35] as factors that could change the amplitude of microwave-radiation-induced magnetoresistance oscillations. Here, we report an experimental study of microwave power and linear polarization angle dependence of the radiation-induced magnetoresistance oscillations, and we compare the results with the predictions of the radiation-driven electron orbit model. The comparison provides new understanding of the experimental results at high microwave powers.

II. THEORETICAL MODEL

The radiation-driven electron orbit model [41,56–58] was developed to explain the observed diagonal resistance, R_{xx}, of an irradiated 2DES at low magnetic field, B, with B in the z direction, perpendicular to the 2DES. Here, electrons behave like a 2D quantum oscillator in the XY plane that contains the 2DES. The system is also subjected to a dc electric field in the x direction ($E_{\rm dc}$), the transport direction, and microwave radiation that is linearly polarized at different angles (θ) with respect to the transport direction (x direction). The radiation electric field is given by $\vec{E}(t) = (E_{0x}\,\vec{i} + E_{0y}\,\vec{j})\cos wt$, where E_{0x} and E_{0y} are the amplitudes of the MW field and w is the frequency. Thus, θ is given by $\tan\theta = \frac{E_{0y}}{E_{0x}}$. The corresponding electronic Hamiltonian can be exactly solved [41,59] obtaining a solution for the total wave function,

$$\Psi(x,y,t) \propto \phi_N[[x - X - a(t)],[y - b(t)],t], \qquad (1)$$

where ϕ_N are Fock-Darwin states, X is the center of the orbit for the electron motion, and $a(t)$ (for the x coordinate) and $b(t)$

(for the y coordinate) are the solutions for a *classical* driven 2D harmonic oscillator (classical uniform circular motion). The expressions for an arbitrary angle θ are given by

$$a(t) = \left[\frac{\sqrt{w^2\cos^2\theta + w_c^2\sin^2\theta}}{w}\right] \times \frac{eE_0\cos wt}{m^*\sqrt{\left(w_c^2 - w^2\right)^2 + \gamma^4}} = A_x\cos wt, \quad (2)$$

$$b(t) = \left[\frac{w\sqrt{w^2\cos^2\theta + w_c^2\sin^2\theta} + \left(w_c^2 - w^2\right)\cos\theta}{ww_c}\right] \times \frac{eE_0\sin wt}{m^*\sqrt{\left(w_c^2 - w^2\right)^2 + \gamma^4}} = A_y\sin wt, \quad (3)$$

where e is the electron charge, γ is a damping factor for the electronic interaction with acoustic phonons, w_c is the cyclotron frequency, and E_0 is the total amplitude of the radiation electric field. These two latter equations give us the equation of an ellipse, $\frac{a^2}{A_x^2} + \frac{b^2}{A_y^2} = 1$. Then, the first finding of this theoretical model is that according to the expressions for $a(t)$ and $b(t)$, the center of the electron orbit performs a classical elliptical trajectory in the XY plane driven by radiation (see the inset of Fig. 4). This is reflected in the x and y directions as harmonic oscillatory motions with the same frequency as radiation. In this elliptical motion, electrons in their orbits interact with the lattice ions being damped and emitting acoustic phonons; in the $a(t)$ and $b(t)$ expressions, γ represents this damping.

The above expressions for $a(t)$ and $b(t)$ are obtained for an infinite 2DES. But if we are dealing with finite samples, the expressions can be slightly different because the edges can play an important role. Then the key issue of symmetry or asymmetry of the sample has to be considered with regard to the polarization sensitivity. In the experiments, the samples were rectangular-shaped or Hall bars (asymmetric samples) and the R_{xx} measurements were obtained at each of the longest sides of the sample between two lateral contacts. According to this experimental setup, we observe that along the classical elliptical trajectories, the driven motion in the x direction presents fewer restrictions since the top and bottom sample edges are far from the R_{xx} measurement points (side contacts). Thus, there are no *spatial* constraints due to the existence of edges. However, for the driven motion in the y direction, the restrictions are very important due to the presence of the edges from the very first moment. The lateral edges impede or make more difficult the MW-driven classical motion of the electron orbits in the y direction. The effect is as if the E_{0y} component of the microwave electric field were much less efficient in coupling and driving the electrons than the E_{0x} component. This situation has to be reflected in the $a(t)$ and $b(t)$ expressions. Thus, we have phenomenologically introduced an asymmetry factor λ to deal with this important scenario affecting the obtained R_{xx}. Since for a more intense radiation electric field E_0 the motion in y is increasingly hindered, we have introduced $\lambda = \frac{1}{1+cE_0}$, where c is a constant that tends to 0 for symmetric samples, and then $a(t)$ reads

$$a(t) = \left[\sqrt{\cos^2\theta + \frac{w_c^2}{w^2}\left(\frac{1}{1+cE_0}\right)\sin^2\theta}\right] \times \frac{eE_0}{m^*\sqrt{\left(w_c^2 - w^2\right)^2 + \gamma^4}}\cos wt = A_x^*\cos wt. \quad (4)$$

This *radiation-driven* behavior has a deep impact on the charged impurity scattering and in turn on the conductivity. Thus, first we calculate the impurity scattering rate $W_{N,M}$ between two driven Landau states Ψ_N and Ψ_M [41,57]. To calculate the electron drift velocity, next we find the average effective distance advanced by the electron in every scattering jump [57]: $\Delta X^{\mathrm{MW}} = \Delta X^0 - A_x^*\sin w\tau$, where τ is the flight time that is strictly the time it takes the electron to go from the initial orbit to the final one. This time is part of the scattering time, τ_S, that is normally defined as the average time between scattering events and equal to the inverse of the scattering rate. ΔX^0 is the average advanced distance without radiation. Finally, the longitudinal conductivity σ_{xx} is given by $\sigma_{xx} \propto \int dE\frac{\Delta X^{\mathrm{MW}}}{\tau_S}$, where E is the energy. To obtain R_{xx}, we use the relation $R_{xx} = \frac{\sigma_{xx}}{\sigma_{xx}^2+\sigma_{xy}^2} \simeq \frac{\sigma_{xx}}{\sigma_{xy}^2}$, where $\sigma_{xy} \simeq \frac{n_i e}{B}$ and $\sigma_{xx} \ll \sigma_{xy}$. Therefore,

$$R_{xx} \propto -\left[\sqrt{\cos^2\theta + \frac{w_c^2}{w^2}\left(\frac{1}{1+cE_0}\right)\sin^2\theta}\right] \times \frac{eE_0}{m^*\sqrt{\left(w_c^2 - w^2\right)^2 + \gamma^4}}\sin w\tau. \quad (5)$$

III. EXPERIMENTS AND RESULTS

Experiments were carried out on high-mobility GaAs/AlGaAs heterostructure Hall bar samples. The samples were placed on a long cylindrical waveguide sample holder and loaded into a variable temperature insert (VTI) inside the bore of a superconducting solenoid magnet. The high-mobility condition was achieved in the 2DES by brief illumination with a red light-emitting diode at low temperature. A microwave launcher at the top of the sample holder excited microwaves within the waveguide sample holder. The angle between the long axis of the Hall bar sample and the antenna in the microwave launcher is defined as the linear polarization angle. This linear polarization angle could be changed by rotating the microwave launcher outside the cryostat. Low-frequency lock-in techniques were utilized to measure the diagonal and off-diagonal response of the sample.

At 1.5 K, the longitudinal resistance R_{xx} versus magnetic field B exhibits strong microwave-radiation-induced magnetoresistance oscillations (see Fig. 1) for frequency $f =$ 45.2 GHz, source power, $P = 4$ mW, and vanishing linear polarization, i.e., $\theta = 0$. The figure shows that maxima and minima up to the fourth order are observable below 0.15 T. The first maxima and minima are designated as $P1$ and $V1$. In Figs. 2 and 3, we examine the linear polarization angle dependence and the microwave power dependence at these extrema.

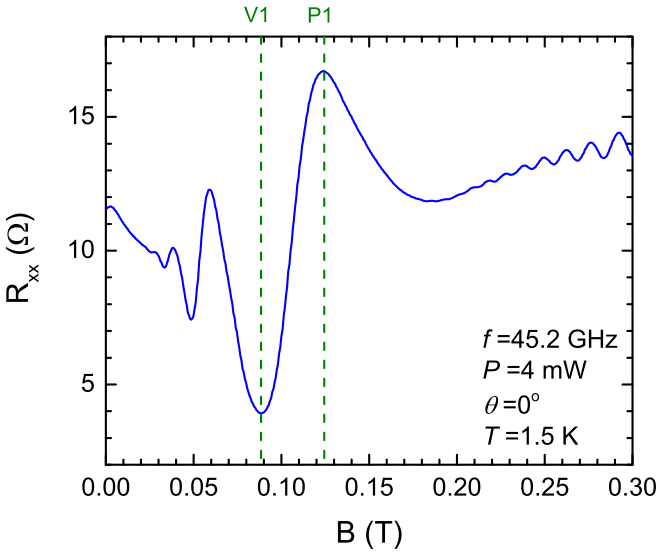

FIG. 1. Longitudinal resistance R_{xx} vs magnetic field B with microwave photoexcitation at 45.2 GHz, 4 mW, and $T = 1.5$ K. The polarization angle, θ, is zero. The labels $P1$ and $V1$ at the top abscissa mark the magnetic fields of the first peak and valley of the oscillatory magnetoresistance.

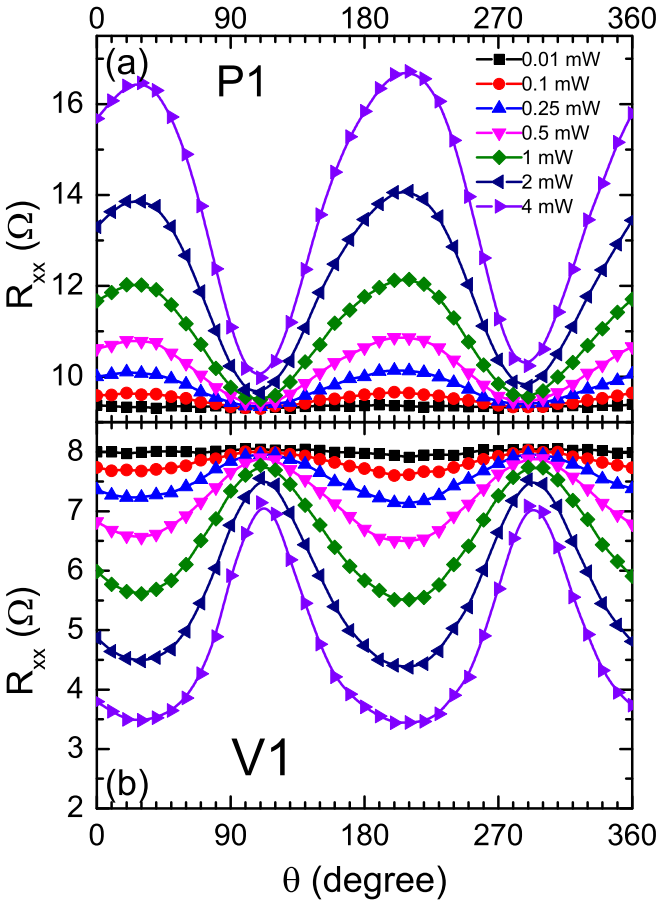

FIG. 2. Longitudinal resistance R_{xx} vs linear polarization angle θ at the magnetic field corresponding to (a) $P1$ and (b) $V1$. The microwave frequency is 42.5 GHz. Different colored symbols represent different source microwave powers from 0 to 4 mW.

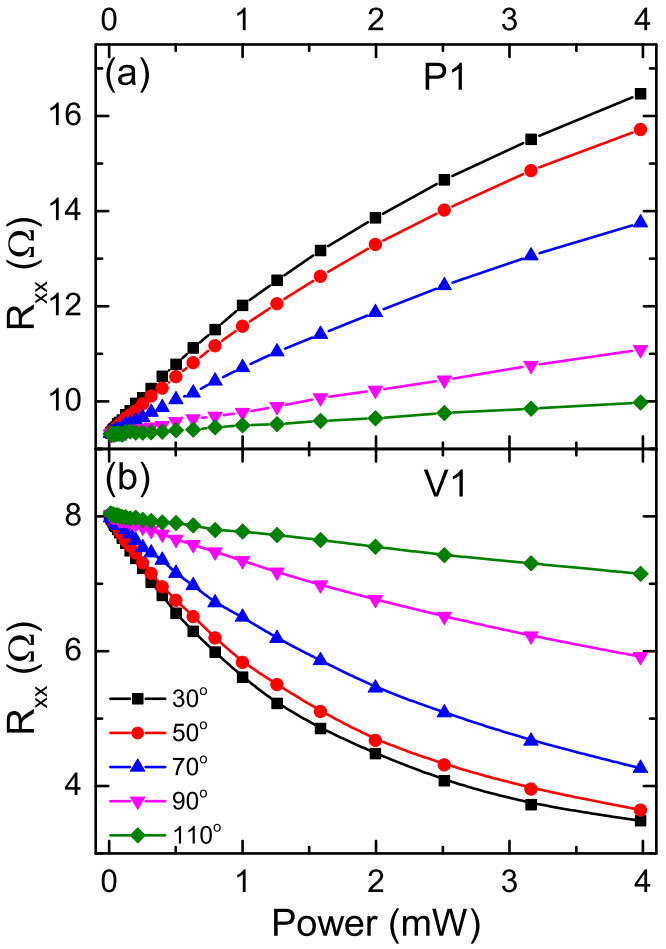

FIG. 3. Longitudinal resistance R_{xx} vs microwave power P at the magnetic field corresponding to (a) $P1$ and (b) $V1$. The microwave frequency is $f = 42.5$ GHz. Different color symbols represent different linear polarization angles, θ, between 30° and 110°.

Figure 2 exhibits R_{xx} versus linear polarization angle θ at different microwave powers at $P1$ and $V1$. The common features of the data at different microwave powers are as follows: (a) they exhibit an oscillatory line shape and (b) the peaks and valleys at all powers occur at the same angle. At low microwave power, the oscillating curve could be represented by a simple sinusoidal function. However, as microwave power increases, the amplitude of the oscillatory curves increases and, at the same time, deviations from the sinusoidal profile become observable and more prominent. For instance, at $P = 4$ mW, the maxima are relatively rounded and the minima are relatively sharp for $P1$, and, in contrast, the maxima are sharp and the minima are rounded for $V1$. At the other oscillatory extrema in the R_{xx} versus B trace at lower B (see Fig. 1), such deviations from simple sinusoidal behavior were more prominent at the same power.

Figure 3 shows R_{xx} versus P at different linear polarization angle θ for $P1$ and $V1$. For $P1$ [see Fig. 3(a)], R_{xx} increases nonlinearly as the microwave power increases. On the other hand [see Fig. 3(b)], R_{xx} decreases nonlinearly with increasing P at $V1$. In Figs. 3(a) and 3(b), all traces start at the same resistance value at $P = 0.01$ mW since the (essentially) dark resistance is invariant under polarization angle rotation.

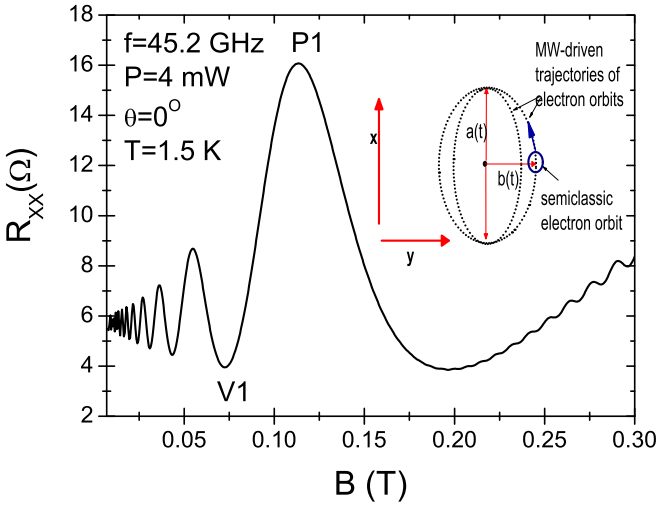

FIG. 4. Calculated irradiated magnetoresistance R_{xx} vs magnetic field B with a microwave frequency of 45.2 GHz, microwave power $P = 4$ mW, and $T = 1.5$ K. The polarization angle, θ, is zero. Symbols $P1$ and $V1$ correspond to the peak and valley, respectively, as indicated.

IV. CALCULATED RESULTS

In Fig. 4, we present calculated results of irradiated R_{xx} versus B for a microwave frequency of 45.2 GHz and power of $P = 4$ mW. As in the experimental curve of Fig. 2, we obtain, at a temperature of $T = 1.5$ K, clear R_{xx} oscillations that turn out to be qualitatively and quantitatively similar to experiment. For the exhibited curve, the polarization angle is zero. The most prominent peak and valley are labeled $P1$ and $V1$, respectively. In the inset of this figure, we present a schematic diagram showing the radiation-driven classical trajectories of the guiding center of the electron orbit.

Figure 5 exhibits calculated results of irradiated R_{xx} versus linear polarization angle θ for different microwave powers for peak $P1$ and valley $V1$ in panels (a) and (b), respectively. The microwave frequency is 45.2 GHz and T is 1.5 K. The microwave power ranges from 0.01 to 6.0 mW. As in the experimental results of Fig. 2, we observe that the R_{xx} curves evolve from a clear sinusoidal profile at low microwave powers to a different profile where, for instance, in the upper panel ($P1$) the peaks broaden and the valleys get sharpened. A similar trend is observable in the lower panel ($V1$). The explanation for this peculiar behavior can be obtained from Eq. (5) and the square root between brackets. When the microwave power (electric-field amplitude E_0) increases, the factor $\frac{w_c^2}{w^2}\left(\frac{1}{1+cE_0}\right)\sin^2\theta$ gets smaller and smaller. As a result, the R_{xx} curve begins to lose its simple sinusoidal profile. At high powers, the latter factor is so small that the $\cos^2$ factor is predominant and the square root tends to the absolute value of $\cos^2$:

$$\left[\sqrt{\cos^2\theta + \frac{w_c^2}{w^2}\left(\frac{1}{1+cE_0}\right)\sin^2\theta}\right] \rightarrow \sqrt{\cos^2\theta} = \text{abs}[\cos\theta]. \quad (6)$$

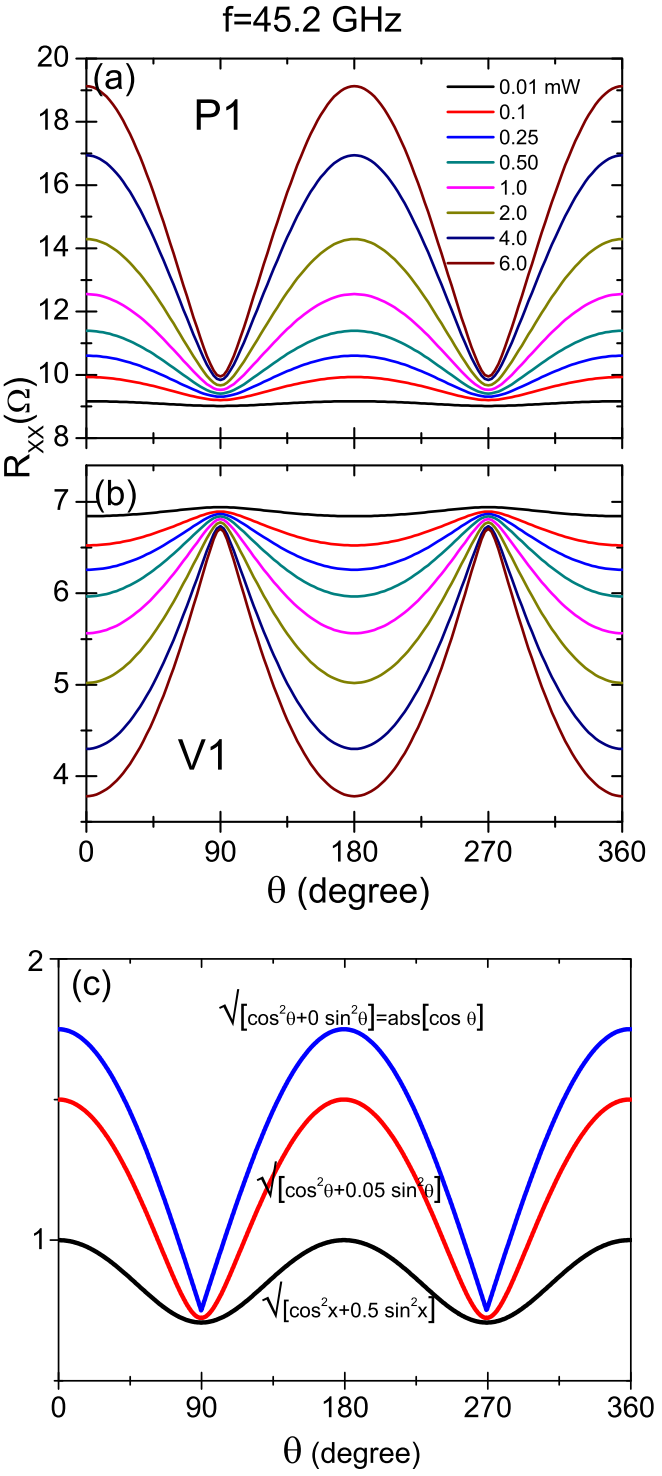

FIG. 5. Calculated irradiated magnetoresistance R_{xx} vs linear polarization angle θ for the magnetic fields corresponding to the peak $P1$ [panel (a)] and valley $V1$ [panel (b)]. In panel (c) we present a simulation of the curves evolution with mathematical functions when the $\sin^2$ term decreases. The microwave photoexcitation is at 45.2 GHz, the microwave power ranges from 0.01 to 6.0 mW, and $T = 1.5$ K.

The profile observed in experiment and calculation for high powers is very similar to that of the abs[cos θ]. This evolution can be clearly observed in Fig. 5(c).

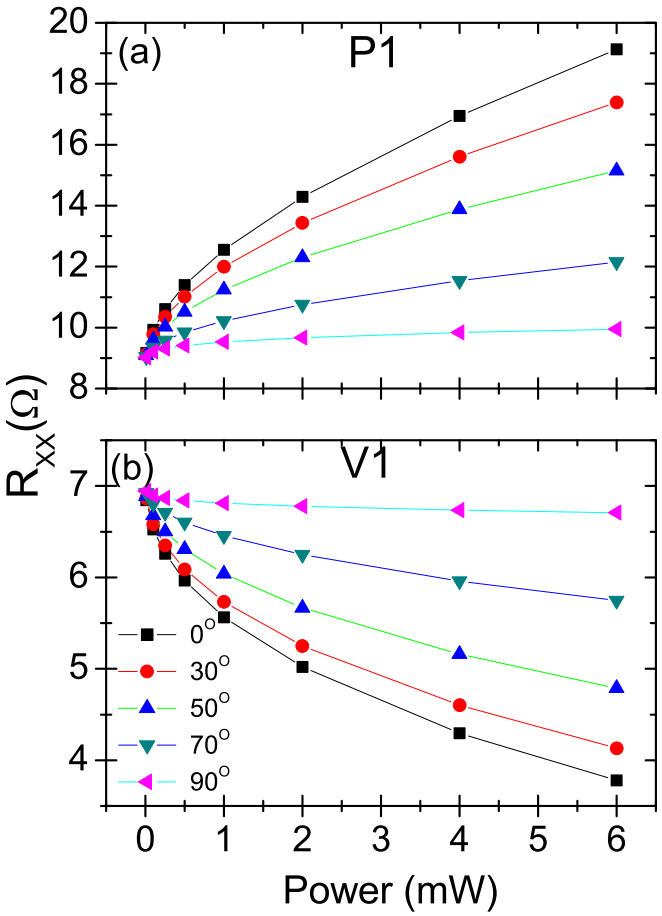

FIG. 6. Calculated irradiated magnetoresistance R_{xx} vs microwave power. The microwave frequency is 45.2 GHz, and $T = 1.5$ K. The polarization angle, θ, ranges from 0° to 90°, as indicated.

In Fig. 6, we present calculated R_{xx} under radiation versus the microwave power for different polarization angles for peak $P1$ (upper panel) and for valley $V1$ (lower panel). For increasing angles from 0° to 90°, the behavior of $P1$ and $V1$ is similar in the sense that the corresponding intensity of both becomes smaller and smaller. In other words, for increasing angles the height of the peak decreases and the depth of the valley decreases too. The theoretical explanation comes from the square-root term as before. For increasing angles the cosine term tends to zero, becoming predominantly the sine term. However, the latter gets smaller with increasing power due to the asymmetry factor. All curves share one important feature, namely that the nonlinearity of R_{xx} versus P suggests a sublinear relation. This behavior can be straightforward explained with our model in terms of

$$E_0 \propto \sqrt{P} \Rightarrow R_{xx} \propto \sqrt{P}. \tag{7}$$

Then the R_{xx} profile with P follows a square-root dependence, as shown by experiments.

V. CONCLUSION

We have presented both experimentally and theoretically calculated results concerning the microwave power and linear polarization angle dependence of the microwave-irradiated oscillatory magnetoresistance in the GaAs/AlGaAs two-dimensional electron system. Experimental results show that, as the microwave power increases, the R_{xx} versus θ traces (see Fig. 2) gradually lose the simple sinusoidal profile, as the profile begins to resemble the absolute value of the cosine function. We presented theoretical insight to explain this evolution using the radiation-driven electron orbit model, which suggests a profile following abs[$\cos\theta$].

Intuitively, one can motivate the change in the profile of the R_{xx} versus θ curves with increasing power by noting that increasing the power, i.e., driving the 2DES more strongly, most likely increases the harmonic content in the R_{xx} versus θ line shape, which leads to deviations from the simple sinusoidal function proposed for low power in Ref. [17]. In the low-power limit, this theoretical prediction of the radiation-driven electron orbit model matched the experimental suggestion of $R_{xx}(\theta) = A \pm C\cos^2(\theta - \theta_0) = A \pm (C/2)\{1 + \cos[2(\theta - \theta_0)]\}$ [17].

One might tie together the low-power R_{xx} versus θ line shape [$\sim\cos^2(\theta)$] with the high-power R_{xx} versus θ line shape (abs[$\cos\theta$]) by examining the Fourier expansion over the interval $[-\pi,\pi]$ of abs[$\cos\theta$] $= (2/\pi) + (4/\pi)\sum_{m=1}^{\infty}\{[(-1)^m/(1-4m^2)]\}\cos(2m\theta)$. If one keeps the lowest-order ($m = 1$) term, which is the only one likely to be observable at low power, then abs[$\cos\theta$] $\rightarrow (2/\pi)[1 + (2/3)\cos(2\theta)] \sim \cos^2(\theta)$.

ACKNOWLEDGMENTS

Magnetotransport measurements and T. Ye at Georgia State University are supported by the U.S. Department of Energy, Office of Basic Energy Sciences, Material Sciences and Engineering Division under DE-SC0001762. Additional support is provided by the ARO under W911NF-15-1-0433 and W911NF-14-2-0076. J.I. is supported by the MINECO (Spain) under Grant No. MAT2014-58241-P and ITN Grant No. 234970 (EU). Grupo de Matematicas Aplicadas a la Materia Condensada (UC3M), Unidad Asociada al CSIC.

[1] R. G. Mani, J. H. Smet, K. von Klitzing, V. Narayanamurti, W. B. Johnson, and V. Umansky, Nature (London) **420**, 646 (2002).

[2] M. A. Zudov, R. R. Du, L. N. Pfeiffer, and K. W. West, Phys. Rev. Lett. **90**, 046807 (2003).

[3] R. G. Mani, W. B. Johnson, V. Umansky, V. Narayanamurti, and K. Ploog, Phys. Rev. B **79**, 205320 (2009).

[4] R. G. Mani, J. H. Smet, K. von Klitzing, V. Narayanamurti, W. B. Johnson, and V. Umansky, Phys. Rev. Lett. **92**, 146801 (2004); Phys. Rev. B **69**, 193304 (2004).

[5] R. G. Mani, C. Gerl, S. Schmult, W. Wegscheider, and V. Umansky, Phys. Rev. B **81**, 125320 (2010).

[6] J. Iñarrea, R. G. Mani, and W. Wegscheider, Phys. Rev. B **82**, 205321 (2010).

[7] A. E. Kovalev, S. A. Zvyagin, C. R. Bowers, J. L. Reno, and J. A. Simmons, Solid State Commun. **130**, 379 (2004).

[8] R. G. Mani, V. Narayanamurti, K. von Klitzing, J. H. Smet, W. B. Johnson, and V. Umansky, Phys. Rev. B **70**, 155310 (2004); **69**, 161306(R) (2004).

[9] B. Simovic, C. Ellenberger, K. Ensslin, H. P. Tranitz, and W. Wegscheider, Phys. Rev. B **71**, 233303 (2005).

[10] R. G. Mani, Phys. Rev. B **72**, 075327 (2005); Appl. Phys. Lett. **85**, 4962 (2004); **91**, 132103 (2007); Physica E **25**, 189 (2004); **40**, 1178 (2008).

[11] S. Wiedmann, G. M. Gusev, O. E. Raichev, T. E. Lamas, A. K. Bakarov, and J. C. Portal, Phys. Rev. B **78**, 121301 (2008).

[12] A. N. Ramanayaka, R. G. Mani, and W. Wegscheider, Phys. Rev. B **83**, 165303 (2011).

[13] R. G. Mani, A. N. Ramanayaka, and W. Wegscheider, Phys. Rev. B **84**, 085308 (2011).

[14] O. M. Fedorych, M. Potemski, S. A. Studenikin, J. A. Gupta, Z. R. Wasilewski, and I. A. Dmitriev, Phys. Rev. B **81**, 201302 (2010).

[15] S. Wiedmann, G. M. Gusev, O. E. Raichev, A. K. Bakarov, and J. C. Portal, Phys. Rev. B **84**, 165303 (2011).

[16] Y. H. Dai, K. Stone, I. Knez, C. Zhang, R. R. Du, C. L. Yang, L. N. Pfeiffer, and K. W. West, Phys. Rev. B **84**, 241303 (2011).

[17] A. N. Ramanayaka, R. G. Mani, J. Iñarrea, and W. Wegscheider, Phys. Rev. B **85**, 205315 (2012).

[18] R. G. Mani, J. Hankinson, C. Berger, and W. A. de Heer, Nat. Commun. **3**, 996 (2012).

[19] T. Ye, R. G. Mani, and W. Wegscheider, Appl. Phys. Lett. **102**, 242113 (2013); **103**, 192106 (2013).

[20] J. Iñarrea, Europhys. Lett. **108**, 27008 (2014).

[21] R. G. Mani, A. Kriisa, and W. Wegscheider, Sci. Rep. **3**, 2747 (2013).

[22] R. G. Mani and A. Kriisa, Sci. Rep. **3**, 3478 (2013).

[23] T. Ye, H. C. Liu, W. Wegscheider, and R. G. Mani, Phys. Rev. B **89**, 155307 (2014).

[24] A. N. Ramanayaka, T. Ye, H. C. Liu, W. Wegscheider, and R. G. Mani, Physica B **453**, 43 (2014).

[25] R. G. Mani, A. N. Ramanayaka, T. Ye, M. S. Heimbeck, H. O. Everitt, and W. Wegscheider, Phys. Rev. B **87**, 245308 (2013).

[26] T. Ye, W. Wegscheider, and R. G. Mani, Appl. Phys. Lett. **105**, 191609 (2014).

[27] H. C. Liu, T. Ye, W. Wegscheider, and R. G. Mani, J. Appl. Phys. **117**, 064306 (2015).

[28] T. Ye, H. C. Liu, Z. Wang, W. Wegscheider, and R. G. Mani, Sci. Rep. **5**, 14880 (2015).

[29] Z. D. Kvon *et al.*, JETP Lett. **97**, 41 (2013).

[30] A. D. Chepelianskii, J. Laidet, I. Farrer, D. A. Ritchie, K. Kono, and H. Bouchiat, Phys. Rev. B **90**, 045301 (2014).

[31] S. Chakraborty, A. T. Hatke, L. W. Engel, J. D. Watson, and M. J. Manfra, Phys. Rev. B **90**, 195437 (2014).

[32] A. D. Levin, Z. S. Momtaz, G. M. Gusev, O. E. Raichev, and A. K. Bakarov, Phys. Rev. Lett. **115**, 206801 (2015).

[33] A. D. Chepelianskii, M. Watanabe, K. Nasyedkin, K. Kono, and D. Konstantinov, Nat. Commun. **6**, 7210 (2015).

[34] X. L. Lei and S. Y. Liu, Phys. Rev. B **86**, 205303 (2012).

[35] J. Iñarrea, J. Appl. Phys. **113**, 183717 (2013).

[36] A. C. Durst, S. Sachdev, N. Read, and S. M. Girvin, Phys. Rev. Lett. **91**, 086803 (2003).

[37] A. V. Andreev, I. L. Aleiner, and A. J. Millis, Phys. Rev. Lett. **91**, 056803 (2003).

[38] V. Ryzhii and R. Suris, J. Phys.: Condens. Matter **15**, 6855 (2003).

[39] A. A. Koulakov and M. E. Raikh, Phys. Rev. B **68**, 115324 (2003).

[40] X. L. Lei and S. Y. Liu, Phys. Rev. Lett. **91**, 226805 (2003).

[41] J. Iñarrea and G. Platero, Phys. Rev. Lett. **94**, 016806 (2005).

[42] I. A. Dmitriev, M. G. Vavilov, I. L. Aleiner, A. D. Mirlin, and D. G. Polyakov, Phys. Rev. B **71**, 115316 (2005).

[43] X. L. Lei and S. Y. Liu, Phys. Rev. B **72**, 075345 (2005).

[44] A. D. Chepelianskii, A. S. Pikovsky, and D. L. Shepelyansky, Eur. Phys. J. B **60**, 225 (2007).

[45] J. Iñarrea, Appl. Phys. Lett. **92**, 192113 (2008).

[46] A. D. Chepelianskii and D. L. Shepelyansky, Phys. Rev. B **80**, 241308 (2009).

[47] J. Iñarrea, Appl. Phys. Lett. **99**, 232115 (2011).

[48] J. Iñarrea, Appl. Phys. Lett. **100**, 242103 (2012).

[49] A. Kunold and M. Torres, Physica B **425**, 78 (2013).

[50] O. V. Zhirov, A. D. Chepelianskii, and D. L. Shepelyansky, Phys. Rev. B **88**, 035410 (2013).

[51] X. L. Lei and S. Y. Liu, J. Appl. Phys. **115**, 233711 (2014).

[52] A. Yar and K. Sabeeh, J. Phys.: Condens. Matter **27**, 435007 (2015).

[53] V. G. Ibarra-Sierra, J. C. Sandoval-Santana, J. L. Cardoso, and A. Kunold, Ann. Phys. (NY) **362**, 83 (2015).

[54] O. E. Raichev, Phys. Rev. B **91**, 235307 (2015).

[55] J. Iñarrea and G. Platero, Nanotechnology **21**, 315401 (2010).

[56] J. Iñarrea and G. Platero, Phys. Rev. B **72**, 193414 (2005).

[57] J. Inarrea and G. Platero, J. Phys.: Condens. Matter **27**, 415801 (2015).

[58] J. Iñarrea, Appl. Phys. Lett. **89**, 052109 (2006).

[59] J. Inarrea and G. Platero, Phys. Rev. B **76**, 073311 (2007).